Wireless Energy Efficiency Evaluation for Buildings Under Design Based on Analysis of Interference Gain

Jiliang Zhang, *Senior Member, IEEE*, Andrés Alayón Glazunov, *Senior Member, IEEE*, and Jie Zhang, *Senior Member, IEEE*

***Abstract*—In this paper, we present part of our ground-breaking work that bridges building design and wireless network deployment. The original contributions lie in: i) defining interference gain (IG) as an intrinsic figure of merit (FoM) of a building's wireless performance in terms of interference signal blockage; ii) developing analytic models to calculate IG; and iii) developing a novel method to calculate the optimum transmitting power to achieve the maximum IG of a building. The IG is derived as an integral transform of the probability density function (PDF) of the distance from a probe user equipment (UE) with a random position relative to a wall, and with a uniformly distributed direction. Furthermore, the PDF of the random distance is derived in closed-form for rectangular rooms to facilitate fast computation of the IG of a building under design (BUD) tiled by rectangular rooms and corridors. For BUD with irregular rooms, a random shooting algorithm (RSA) is proposed to numerically compute the PDF. The closed-form expression and the RSA are compared and validated. Numerical results show the validity of both the model to calculate IG and the methodology to derive the optimum transmitting power to achieve the maximum IG of a given building. The results shed light to architects on how to design buildings with desirable wireless performance and for radio engineers on how densely wireless access points can be deployed to approach the intrinsic wireless performance of a building.**

***Index Terms*—Smart buildings, building design, wireless performance evaluation, 5G networks.**

I. Introduction

Wireless communication networks play an important role in the design of smart buildings [1], [2], or more broadly, in the practical realization of smart cities [3]. It has been estimated that nearly 80% of data traffic occurs indoors [4]. In future 5G indoor networks, transmit elements, e.g., access points or small cell base stations, are expected to be ultra-densely deployed [5]–[7] to improve quality of service (QoS), e.g., in terms of data throughput and latency. With ultra-densely deployment, power consumption of an indoor wireless network has to be taken into account carefully [8].

Traditionally, research on indoor wireless networks performance has focused on indoor propagation channel modelling [9]–[14], random blockage modelling [15]–[17], and line-of-sight (LOS) probability analysis [18]–[21], etc. Analysis on indoor network performances has therefore shed light on the impact of building structures on specific wireless networks performance.

We have previously proposed the idea that every building has an intrinsic wireless performance which is independent of how densely small cells are deployed [22]. The above idea suggests that a building can be designed and built taking into account its intrinsic wireless communication performance. Therefore, if a building is designed by considering its intrinsic wireless communication performance considerable cost reduction can be achieved since there will be no need to go through costly and inconvenient modification/retrofitting in the future. However, how to design buildings to achieve a desirable wireless performance has never been systematically researched. To address the challenging evaluation of building wireless communication (BWC) performance, the collaborative project Build-Wise has been granted under the open call of Eurostars programme [23]. It is worth noting that both building layouts and building materials have impacts on the BWC. In this paper, we only focus on the impact of the building layout in the first stage, while the impact of materials has been left for our future work.

Supported by the project, [22] proposed a framework to evaluate the wireless performance of the layout of the buildings under design (BUD) by using the open space scenario as a benchmark. Therein, two figures of merit (FoM) have been defined: (i) the interference gain (IG) and (ii) the power gain (PG), both reflecting the BWC performance. In this paper, we focus on the analysis of IG, which captures the impact of the building layout on the power of interference signals due to blockage by building structures. The definition of IG will be provided in subsection II-A.

In [22], the proposed IG is determined not only by the layout of the BUD, but also by parameters of the wireless network, e.g., the transmit power, sensitivity of the receiver, operating frequency band, and positions of probe UEs. The objective of the FoM is to provide either architects or wireless communication engineers with guidance regarding the impact of the building layout on the BWC performance.

Manuscript received May 30, 2019; revised October 15, 2019, February 12, 2020, and March 29, 2020; accepted March 30, 2020. Date of publication April 6, 2020; date of current version June 18, 2020. The work was supported by EUROSTARS Project BuildWise (11088). The review of this article was coordinated by Prof. D. Benevides da Costa. *(Corresponding author: Jie Zhang.)*

Jiliang Zhang is with the Department of Electronic and Electrical Engineering, The University of Sheffield, Sheffield S10 2TG, U.K. (e-mail: jiliang.zhang@sheffield.ac.uk).

Andrés Alayón Glazunov is with the Department of Electrical Engineering, University of Twente, 7522 Enschede, The Netherlands, and also with the Department of Electrical Engineering, Chalmers University of Technology, 412 96 Gothenburg, Sweden (e-mail: a.alayonglazunov@utwente.nl).

Jie Zhang is with the Department of Electronic and Electrical Engineering, The University of Sheffield, Sheffield S10 2TG, U.K., and also with the Ranplan Wireless Network Design Ltd., Cambridge CB23 3UY, U.K. (e-mail: jie.zhang@sheffield.ac.uk).

Digital Object Identifier 10.1109/TVT.2020.2985615

0018-9545 © 2020 IEEE. Personal use is permitted, but republication/redistribution requires IEEE permission.
See https://www.ieee.org/publications/rights/index.html for more information.

In order to facilitate the analysis, the impacts of building layouts and parameters of wireless networks have to be decoupled into two independent factors. Moreover, the question of how much energy should be used to achieve a desirable IG is a fundamental question to be tackled in order to obtain an optimal BWC performance. To approach the objective, we evaluate the energy efficiency of a building by separating the impact of the building layout and the parameters of wireless networks in the computation of IG. The contributions of this paper are summarized as follows.

- The individual contributions of parameters of wireless networks and parameters of building layouts into the computing of the interference gain (IG) are decoupled the one from the other. The IG is computed by an integral transform of the probability density function (PDF) of the LOS distance that is defined as the distance from a probe UE with a random position to the wall in a uniformly distributed random direction. The piecewise kernel function of the integral transform is only determined by parameters of the wireless network, and the LOS-distance PDF only depends on the layout of the BUD.
- The maximum ratio between IGs of the BUD and a small benchmark room is introduced to evaluate the BWC performance of the BUD. The optimum transmitting power achieving the maximum IG ratio is obtained by solving an integral equation.
- The LOS-distance PDF is derived in closed-form for rectangular rooms to facilitate the fast computation of the IG of a building tiled by rectangular rooms and corridors. For buildings with irregular rooms, a random shooting algorithm (RSA) is proposed to numerically compute the LOS-distance PDF. The closed-form expression and the RSA are compared showing excellent agreement.
- Finally, the network power consumption in terms of transmit power that achieves an optimum IG of the BUD is derived.

The remainder of this paper is organized as follows. In Section II, assumptions and definitions used in this paper are stated. In Section III, decoupling of parameters of wireless networks and parameters of building layouts. In Section IV, the maximum IG ratio is defined as a FoM of BWC performance. Using this definition, we optimize the transmitting power to achieve the best IG of a given BUD. In Section V, a derivation method is outlined for the LOS-distance PDF of the distance from a probe UE with a random position to the wall in a random direction. Section VI provides numerical results, and Section VII concludes this paper.

II. Model and Figure of Merit

A. Definition of IG

In this paper, we focus on the analysis of interference gain, which is employed to measure the impact of building structure on the power of interference signals due to blockage. In a wireless network, the received signal is contaminated by the noise and interference. We denote the power of the interference signal in the open space as I_{O}. The power of the interference signal in the BUD at a given position (x, y) is denoted by $I_{\mathrm{B}}(x, y)$. The parameter σ^2 denotes the variance of the noise. Then, the metric IG can be defined as the ratio of the noise and interference between the open space and the built environment, i.e.,

$$g_{\mathrm{I}}(x, y) \triangleq \frac{I_{\mathrm{O}} + \sigma^2}{I_{\mathrm{B}}(x, y) + \sigma^2}. \tag{1}$$

From (1), we can see that a greater IG means that more interference is blocked by the building structure. Therefore, we need to target a greater IG during the building-design stage.

Based on the definition of IG for a specific indoor position, the IG for a building that consists of N_{r} rooms is given by

$$g_{\mathrm{I}} \triangleq \mathrm{E}_{(x,y)\in \mathrm{BUD}}\left[g_{\mathrm{I}}(x, y)\right] = \sum_{n_{\mathrm{r}}=1}^{N_{\mathrm{r}}} \frac{S_{n_{\mathrm{r}}} g_{\mathrm{I}, n_{\mathrm{r}}}}{S_{\mathrm{A}}}, \tag{2}$$

where $g_{\mathrm{I},n_{\mathrm{r}}} \triangleq \mathrm{E}_{(x,y)\in n_{\mathrm{r}}\text{th room}}[g_{\mathrm{I}}(x, y)]$ denotes the IG of the n_{r}th room, $S_{n_{\mathrm{r}}}$ denotes the floor area of the n_{r}th room, and $S_{\mathrm{A}} = \sum_{n_{\mathrm{r}}=1}^{N_{\mathrm{r}}} S_{n_{\mathrm{r}}}$ denotes the area of the BUD.

B. System Model for IG Compuation

Assumption 1: We assume that small cells are extremely densely distributed in the environment in this paper.

In particular, the small cells, each of which has an infinitesimal transmit power, are deployed with infinitesimal cell size.

Assumption 2: Interference-limited networks are investigated where the noise is negligible.

According to [32, Definition 10], the aggregate interference is extremely large compared with the noise when the density of the small-cell network is infinitely large. Therefore, this paper focuses on interference-limited ultra-dense cellular networks as in [33]–[35], where the noise becomes negligible. Then, the IG is only determined by the interference signals

$$g_{\mathrm{I}}(x, y) \triangleq \frac{I_{\mathrm{O}}}{I_{\mathrm{B}}(x, y)}, \tag{3}$$

where we have assumed that $I_{\mathrm{B}}(x, y) >> \sigma^2$ and $I_{\mathrm{O}}(x, y) >> \sigma^2$. According to (3), $g_{\mathrm{I}} \geq 0$, and is determined by both I_{O} and I_{B}.

Assumption 3: The probe UE can make use of all the detectable power, which is constrained by the sensitivity of its receiver.

In an infinitely dense small-cell network, the transmit power of each small cell, with an infinitesimal size of $\mathrm{d}A$, is also infinitesimal and given by $P_{\mathrm{T}}\mathrm{d}A$, where the parameter P_{T} $[\mathrm{Wm}^{-2}]$ denotes the transmit power per unit area. Then in an arbitrary plane surface domain with an area A, the total transmit power from small cells within this space is $P_{\mathrm{T}}A$. Because of the propagation attenuation, the received power of the probe UE from a small cell is then $P_{\mathrm{T}}\mathrm{d}AG_s(R)$ [W], which is an infinitesimal, too, where $s \in \{\mathrm{O}, \mathrm{L}, \mathrm{N}\}$, and $G_{\mathrm{O}}(R)$, $G_{\mathrm{L}}(R)$, and $G_{\mathrm{N}}(R)$ are the path gain of the wireless propagation channel in open space, in the LOS, and in the non-line-of-sight (NLOS) scenarios, respectively. Then, the UE can make use of all the detectable power that is greater than a threshold power level. The threshold power level at the receiver is also infinitesimal and proportional to $\mathrm{d}A$, let's say $P_{\mathrm{th}}\mathrm{d}A$ [W], and P_{th} has the unit $[\mathrm{Wm}{-2}]$. Then, the cumulative undetectable power, which is calculated as the summation of received power that is lower than the threshold power level, is considered as interference. More specifically, the interference power is defined as the total received power from small cells satisfying

$$P_{\mathrm{T}} G_s(R) < P_{\mathrm{th}}, s \in \{\mathrm{O}, \mathrm{L}, \mathrm{N}\}, \tag{4}$$

where R [m] denotes the distance from a small cell to the probe UE, and P_{th} $[\mathrm{Wm}^{-2}]$ is the threshold determined by the sensitivity of the receiver.

C. Bounded Path Gain Models

Assumption 4: Bounded path gain models for the open space, the LOS and the NLOS scenarios are employed in this paper.

For the open space scenario, the path gain is given by [24, Eqs. (4), (5)]

$$G_{\mathrm{O}}(R) = \min\left\{1, \left(\frac{\lambda}{4\pi}\right)^2 R^{-2}, (h_{\mathrm{T}} h_{\mathrm{R}})^2 R^{-4}\right\}, \tag{5}$$

where λ [m] is the wavelength at the center operating frequency. h_{T} [m] and h_{R} [m] denote height of transmit and receive antennas, respectively. For the LOS and the NLOS scenarios, the path gain is given by [25], [26]

$$G_{\mathrm{L}}(R) = \begin{cases} G_{\mathrm{O}}(R), & R \leq 1, \\ \left(\frac{\lambda}{4\pi}\right)^2 R^{-n_{\mathrm{L}}}, & R > 1, \end{cases} \tag{6}$$

$$G_{\mathrm{N}}(R) = \begin{cases} G_{\mathrm{O}}(R), & R \leq 1, \\ \left(\frac{\lambda}{4\pi}\right)^2 R^{-n_{\mathrm{N}}}, & R > 1, \end{cases} \tag{7}$$

where n_{L} and n_{N}, respectively, denote the path loss exponents (PLE) of the LOS and NLOS propagation scenarios, which depend on the building materials. The path gain for NLOS propagation contains not only the distance-dependent loss but the attenuation due to blockage effects. The received power is greater in a in LOS link than in a NLOS link with the same link length, and thus the PLE of NLOS propagation is greater than that of LOS propagation since $n_{\mathrm{N}} > n_{\mathrm{L}}$. The presented approaches in this paper are applicable for arbitrary $n_{\mathrm{L}} > 1$ and $n_{\mathrm{N}} > 2$.

We define the coverage distance $R_s, s \in \{\mathrm{O}, \mathrm{L}, \mathrm{N}\}$ as the distance satisfying $P_{\mathrm{T}} G_s(R_{\mathrm{s}}) = P_{\mathrm{th}}$, where O, L, and N denote open space transmission, LOS transmission and NLOS transmission, respectively. For any small cell, when the link to the probe UE satisfies the condition s, and the distance between the small cell and the probe UE is greater than the coverage distance R_{s}, the signal transmitted from the small cell is considered as an interference signal for the probe UE. Otherwise, if the distance between the small cell and the probe UE is smaller than R_{s}, the signal transmitted from the small cell is considered as an intended signal and can be used to convey information. After some straightforward algebraic manipulations we obtain that

$$R_{\mathrm{O}} = \begin{cases} \sqrt{\rho}, & \rho < \frac{(4\pi)^2 (h_{\mathrm{T}} h_{\mathrm{R}})^2}{\lambda^2}, \\ \rho^{\frac{1}{4}} \sqrt{\frac{4\pi h_{\mathrm{T}} h_{\mathrm{R}}}{\lambda}}, & \rho \geq \frac{(4\pi)^2 (h_{\mathrm{T}} h_{\mathrm{R}})^2}{\lambda^2}, \end{cases} \tag{8}$$

$$R_{\mathrm{L}} = \rho^{\frac{1}{n_{\mathrm{L}}}}, \tag{9}$$

$$R_{\mathrm{N}} = \rho^{\frac{1}{n_{\mathrm{N}}}}, \tag{10}$$

where the effective transmit signal-to-threshold ratio ρ is defined by

$$\rho \triangleq \left(\frac{P_{\mathrm{T}}}{P_{\mathrm{th}}}\right) \left(\frac{\lambda}{4\pi}\right)^2. \tag{11}$$

ρ is proportional to the transmit power per coverage area P_{T}. It follows from (8)-(10) that the value of $R_{\mathrm{O/L/N}}$ is irrelevent to specific values of $(P_{\mathrm{T}}, P_{\mathrm{th}}, \lambda)$ as long as the value of ρ is provided. In particular, different values of $(P_{\mathrm{T}}, P_{\mathrm{th}}, \lambda)$ with a same value of ρ lead to a same $R_{\mathrm{O/L/N}}$.

D. Computation of IG

Assumption 5: In cooperative ultra-dense small-cell/massive MIMO systems, channel responses are smoothed by the law of large numbers. In essence, small-scale fading is negligible. Therefore, only large-scale fading is considered in this paper.

The density of transmitters is extremely high and the overall effect interference is the summation of interfering power from uniformly distributed transmitters that spread over the area. In the open space propagation scenario, the interference power is given by

$$I_{\mathrm{O}} = \int_0^{2\pi} \int_{R_{\mathrm{O}}}^{+\infty} P_{\mathrm{T}} G_{\mathrm{O}}(R) \mathrm{d}R \mathrm{d}\theta. \tag{12}$$

Substituting (5) and (11) into (12), we obtain

$$I_{\mathrm{O}} = \begin{cases} P_{\mathrm{T}} \left[\frac{1}{2} + \ln\left(\frac{4\pi h_{\mathrm{T}} h_{\mathrm{R}}}{\sqrt{\rho}\lambda}\right)\right] \frac{\lambda^2}{8\pi}, & 1 < \rho < \rho_{\mathrm{t}}, \\ P_{\mathrm{T}} h_{\mathrm{T}} h_{\mathrm{R}} \frac{\lambda}{4\sqrt{\rho}}, & \rho \geq \rho_{\mathrm{t}}, \end{cases} \tag{13}$$

where $\rho_{\mathrm{t}} = \frac{(4\pi h_{\mathrm{T}} h_{\mathrm{R}})^2}{\lambda^2}$ is the break point of the I_{O} caused by the break point in the piece-wise function $G_{\mathrm{O}}(R)$ at $R = \frac{4\pi h_{\mathrm{T}} h_{\mathrm{R}}}{\lambda}$.

Whereas in the BUD, the interference power is given by

$$I_{\mathrm{B}}(x, y) = \underbrace{\int_{\mathcal{V}(r,R,\theta)\wedge(R \geq R_L)} P_{\mathrm{T}} G_{\mathrm{L}}(R) \mathrm{d}R \mathrm{d}\theta}_{I_{\mathrm{L}}} + \underbrace{\int_{\neg\mathcal{V}(r,R,\theta)\wedge(R \geq R_N)} P_{\mathrm{T}} G_{\mathrm{N}}(R) \mathrm{d}R \mathrm{d}\theta}_{I_{\mathrm{N}}}, \tag{14}$$

where I_{L} and I_{N} denote the LOS and the NLOS received powers of interference signal, respectively. The Boolean variable $\mathcal{V}(r, R, \theta)$ denotes that the proposition "the link from the small cell at (R, θ) to the probe UE position $r = (x, y)$ is LOS" is true.

Then, the IG is obtained by substituting (13) and (14) into (3). Given $(\lambda, h_{\mathrm{T}}, h_{\mathrm{T}}, n_{\mathrm{L/N}})$, since both I_{O} and I_{B} are proportional to P_{T}, the IG for the location r is determined only by the value of ρ, which is the only variable that is related to P_{T} in the computation. Therefore, the optimization of P_{T} is equivalent to the optimization of ρ.

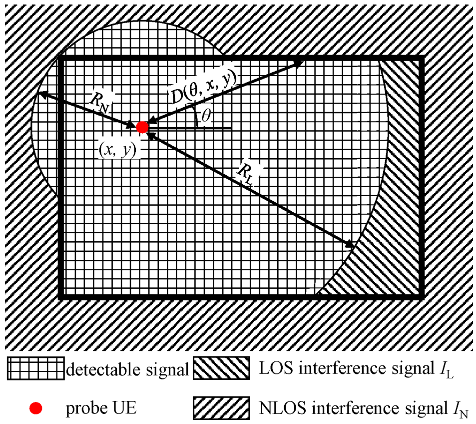

Fig. 1. Coordinate and definition of D. The probe UE receives signals from all small cells that span over the whole 2D Euclidean plane. If the distance from a small cell in the LOS/NLOS region is greater than $R_{\mathrm{L/N}}$, the signal is not detectable by the UE and is considered as an interference signal. Otherwise, if the distance from a small cell in the LOS/NLOS region is smaller than $R_{\mathrm{L/N}}$, the signal is considered as a detectable signal. The summation of all interference signals are defined as I_{B}, which is computed by (14).

Given an optimized ρ that maximizes the IG, the corresponding transmit power per coverage area P_{T} can be computed straightforwardly from (11) as

$$P_{\mathrm{T}} = \rho P_{\mathrm{th}} \left(\frac{4\pi}{\lambda}\right)^2. \quad (15)$$

Remark 1: Through (1)–(15), we can see that parameters which determine the value of IG can be classified as building layout parameters and wireless networks parameters. The parameters of building layouts are the possible position of probe UEs (x, y), and the Boolean variable $\mathcal{V}(r, R, \theta)$ for all possible probe UE positions. Parameters of wireless networks include the transmit power density P_{T}, the sensitivity of receiver P_{th}, the considered wave length λ, the PLE n_s, and the height of BS and UE antennas h_{T} and h_{R}, respectively. Using the definition in (11), P_{T}, P_{th}, and λ are combined into one parameter, i.e., ρ. In the next section, contributions of building layouts and wireless networks will be decoupled to separately analyze their contributions to the IG of buildings.

E. Impact of IG on Performance of Indoor Wireless Networks

In this subsection, the impact of the IG, the metric defined to evaluate the wireless performance of building layout, on the interference of indoor wireless networks are illustrated. To give an example, IG is obtained in a rectangular room with a size of 5 m $\times$ 10 m. Three probe UEs, i.e., UE A $(-2, -3)$, UE B $(-2,0)$ and UE C $(0,0)$, are considered, as shown in Fig. 2(a). The numerical results are obtained at 1GHz band, where $P_{\mathrm{T}} = -30$ dBW/m^2, $P_{\mathrm{th}} = -75$ dBW/m^2, $n_{\mathrm{L}} = 1.73$, $n_{\mathrm{N}} = 3.19$, and $h_{\mathrm{T}} = h_{\mathrm{R}} = 1.2$ m. According to (11), $\rho = 18$. According to (9) and (10), the coverage distance are computed as $R_{\mathrm{L}} = 5.3$ m and $R_{\mathrm{N}} = 2.5$ m, respectively. Following (3), IGs of the building layout for probe UEs A, B and C are 9.9, 13.8, and 16.3, respectively. The probe UE C achieves the highest IG because most of the interference signals are blocked by the building structures while majority of strong LOS signals are detectable. The probe UE A achieves the lowest IG because it receives a relatively large number of strong LOS interference signals.

To show the impact of the IG on the performance of specific networks, the simulations are carried out for two typical indoor networks, i.e., the Poisson point process (PPP) and the grid networks [33]. In the PPP indoor network, BSs are Poisson distributed in the environment, as shown in Fig. 2(b-d). In the grid indoor network, BSs are located on a square lattice in the environment, as shown in Fig. 2(e-g). In the simulation, the intensity of both the PPP and the grid networks are set as 0.5 BSs/m^2. According to the definition of P_{T} in Assumption 3, each BS has a transmit power of -27 dBW. Following above assumptions, we plot the ratios of interference powers under the open space and the indoor environment in Fig. 2(h). Numerical results show that the ratios of interference powers for both PPP and grid networks converge to the IG with an increasing network intensity. According to this observation, we assume that the ratios of interference powers of practical networks converge to the IG as well. Therefore, we can conclude that the IG captures the impact of building structures on the interference of ultra-dense small cell networks. In the following sections, we will investigate how much power do we need to efficently increase the IG of the building layout.

III. Decoupling of Network Parameters and Building Layouts

In (3), IG is computed via I_{O} and I_{B}, where I_{O} is computed by (13) straightforwardly. For the computation of I_{B}, we propose the following Proposition 1.

Proposition 1: The power I_{B} can be computed by

$$I_{\mathrm{B}}(x, y) = \int_0^{+\infty} I_{\mathrm{B},0}(d, \rho, n_{\mathrm{L}}, n_{\mathrm{N}}, P_{\mathrm{th}}) P_D(d; x, y) \mathrm{d}d, \quad (16)$$

$$I_{\mathrm{B},0}(D, \rho, n_{\mathrm{L}}, n_{\mathrm{N}}, P_{\mathrm{th}}) = \underbrace{\frac{2\pi P_{\mathrm{th}} u\left[D - \rho^{\frac{1}{n_{\mathrm{L}}}}\right]\left[D^{2-n_{\mathrm{L}}}\rho - \rho^{\frac{2}{n_{\mathrm{L}}}}\right]}{2 - n_{\mathrm{L}}}}_{I_{\mathrm{L},0}} - \underbrace{\frac{2\pi P_{\mathrm{th}} \rho \max\{D, \rho^{\frac{1}{n_{\mathrm{N}}}}\}^{2-n_{\mathrm{N}}}}{2 - n_{\mathrm{N}}}}_{I_{\mathrm{N},0}} \quad (17)$$

$$I_{\mathrm{B},0}(D, \rho, n_{\mathrm{L}}, n_{\mathrm{N}}, P_{\mathrm{th}}) = 2\pi P_{\mathrm{th}} \begin{cases} \frac{D^{2-n_{\mathrm{N}}}\rho}{n_{\mathrm{N}}-2} + \frac{D^{2-n_{\mathrm{L}}}\rho - \rho^{\frac{2}{n_{\mathrm{L}}}}}{2-n_{\mathrm{L}}}, & D > R_{\mathrm{L}} \\ \frac{D^{2-n_{\mathrm{N}}}\rho}{n_{\mathrm{N}}-2}, & R_{\mathrm{N}} < D \le R_{\mathrm{L}} \\ \frac{\rho^{\frac{2}{n_{\mathrm{N}}}}}{n_{\mathrm{N}}-2}, & D \le R_{\mathrm{N}} \end{cases} \quad (18)$$

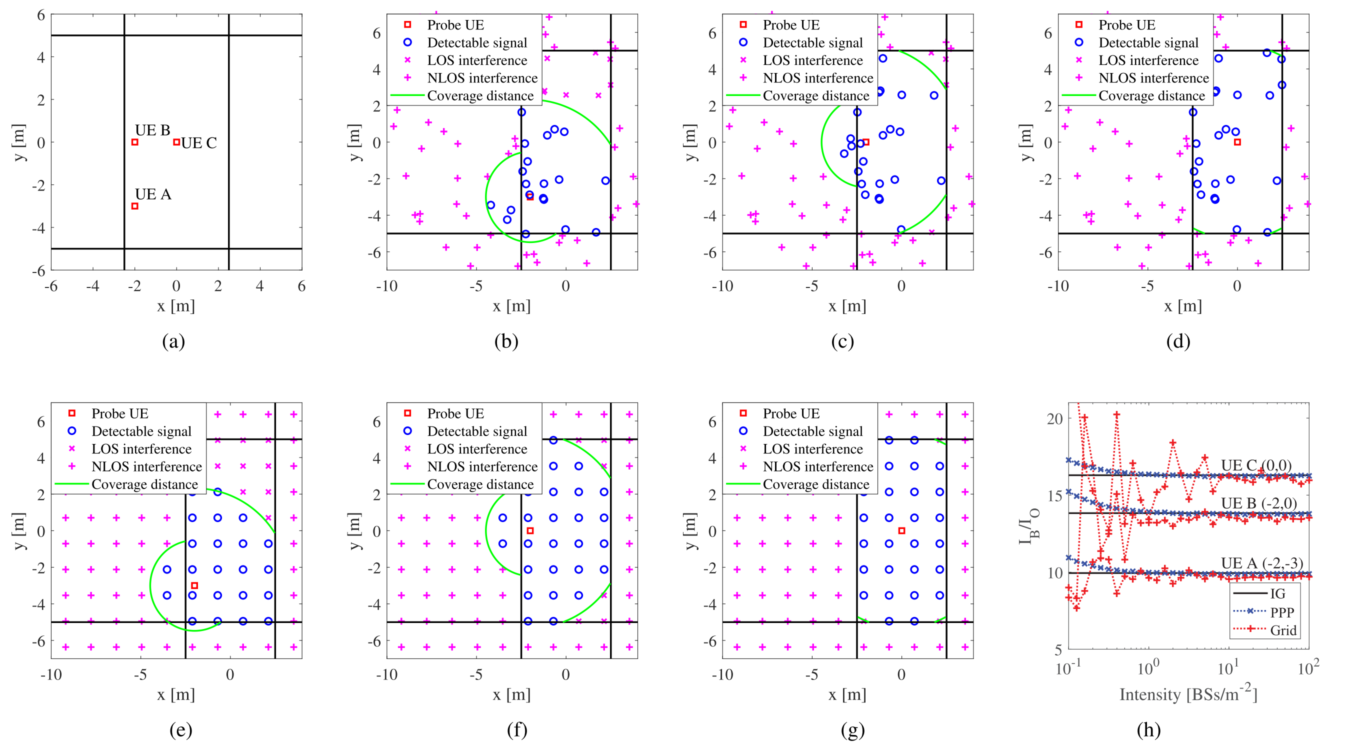

Fig. 2. The impact of building structures on the interference power of PPP and grid small-cell networks while probe UEs are located in a rectangular room. In this example, the size of the considered room is 5 m × 10 m, and three probe UEs, i.e., UE A (−2, −3), UE B (−2, 0) and UE C (0, 0), are observed. Numerical results show that the ratios of interference powers for both PPP and grid networks converge to the IG with an increasing network intensity. The curves for the PPP network are smoothed by averaging simulation results. In contrast, curves of the grid network varys rapidly because the BSs of grid networks are not randomly distributed and the interference power ratio can not be smoothed by averaging simulation results. (a) Probe UEs. (b) UE A, PPP. (c) UE B, PPP. (d) UE C, PPP. (e) UE A, grid. (f) UE B, grid. (g) UE C, grid. (h) Power ratios and IG.

where the LOS-distance D is the distance from a probe UE at a random position (x, y) to the wall in an uniformly distributed direction θ. $P_D(d)$ is the PDF of D. For a given position of the probe UE given by coordinates (x, y) on the horizontal plane and a given direction θ (an example of $D(\theta, x, y)$ is illustrated in Fig. 1). $I_{\mathrm{B},0}(D, \rho, n_{\mathrm{L}}, n_{\mathrm{N}}, P_{\mathrm{T}})$ denotes the received interference power assuming that the distance from the probe UE to the wall in all directions is D. Eq. (16) indicates that $I_{\mathrm{B}}(x, y)$ is the expected value of $I_{\mathrm{B},0}(d, \rho, n_{\mathrm{L}}, n_{\mathrm{N}}, P_{\mathrm{th}})$ for by given position of the probe UE with coordinates (x, y). $I_{\mathrm{B},0}(D, \rho, n_{\mathrm{L}}, n_{\mathrm{N}}, P_{\mathrm{T}})$ is given in closed-form by (17) shown at the bottom of the previous page, where $u(x)$ is the Heaviside step function. Written as a piecewise function, $I_{\mathrm{B},0}(D, \rho, n_{\mathrm{L}}, n_{\mathrm{N}}, P_{\mathrm{T}})$ is given by (18) shown at the bottom of the previous page.

Proof: A proof is provided in Appendix A. It makes use of Lemmas 2 and 3 presented further below. ∎

Remark 2: It is worthwhile to note that $I_{\mathrm{B}}(x, y)$ is computed by two functions, i.e., $I_{\mathrm{B},0}$ and $P_D(D; x, y)$, where $I_{\mathrm{B},0}$ is determined by the parameters of the indoor wireless network, while $P_D(D; x, y)$ is determined by the layout of the BUD and the position of the probe UE.

In order to exemplify how the above proposition works in practice, we specialize our results to numerical parameters of a generic indoor wireless network. For $P_{\mathrm{T}} = -20\ \mathrm{dBWm}^{-2}$, $P_{\mathrm{th}} = -110\ \mathrm{dBWm}^{-2}$, $f = 28$ GHz, $I_{\mathrm{B},0}(D, \rho, n_{\mathrm{L}}, n_{\mathrm{N}}, P_{\mathrm{th}})$ is plotted in Fig. 4, from which it can be seen that

- If $D < R_{\mathrm{N}}$, then $I_{\mathrm{B},0}(D, \rho, n_{\mathrm{L}}, n_{\mathrm{N}}, P_{\mathrm{th}})$ is independent from D because all the power of the NLOS interference from a small cell satisfying $R > R_{\mathrm{N}}$ is received by the probe UE regardless of the value of D. Thus, $I_{\mathrm{N},0}$ is a constant in this scenario. Furthermore, since $D < R_{\mathrm{L}}$ also holds in this case, we have $I_{\mathrm{L},0} = 0$. Therefore, if the room is extremely small such that $P_D(D; x, y) = 0$ for all $D > R_{\mathrm{N}}$, $I_{\mathrm{B},0}(D, \rho, n_{\mathrm{L}}, n_{\mathrm{N}}, P_{\mathrm{th}})$ only depends on ρ.
- If $R_{\mathrm{N}} < D < R_{\mathrm{L}}$, then $I_{\mathrm{B},0}(D, \rho, n_{\mathrm{L}}, n_{\mathrm{N}}, P_{\mathrm{th}})$ decreases with increasing D because more NLOS interference power is blocked, whereas all signals are considered as detectable power in the LOS regime, i.e., $I_{\mathrm{L},0} = 0$.
- However, if $D > R_{\mathrm{L}}$, then $I_{\mathrm{B},0}(D, \rho, n_{\mathrm{L}}, n_{\mathrm{N}}, P_{\mathrm{th}})$ dramatically increases with an increasing D due to the strong interference from the LOS small cells. For a large room or a small ρ, the increasing power of LOS interference increases $I_{\mathrm{B},0}(D, \rho, n_{\mathrm{L}}, n_{\mathrm{N}}, P_{\mathrm{th}})$ and therefore reduces the IG significantly.

Fig. 3 shows $I_{\mathrm{B},0}(D)$ for various values of ρ. With an increasing ρ, the transmit power of NLOS interference small cell increases too, which in turn leads to the increasing of $I_{\mathrm{B},0}(D, \rho, n_{\mathrm{L}}, n_{\mathrm{N}}, P_{\mathrm{th}})$ and a reducing of g_{I}. Nevertheless, when ρ increases, R_{L} becomes larger and therefore less LOS interference is received by the probe UE for a given D. Then, g_{I} could be reduced by increasing ρ significantly. Therefore, to achieve an optimum g_{I}, ρ has to be chosen carefully: 1) to block

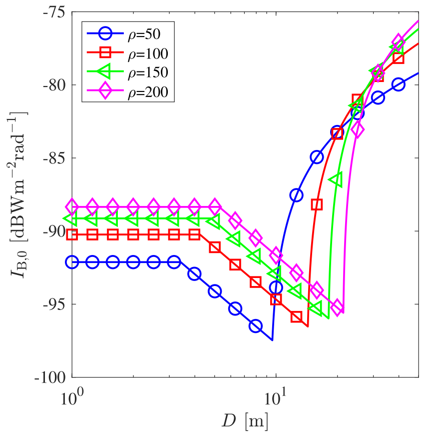

Fig. 3. $I_{\mathrm{B},0}$ for various ρ, where $n_{\mathrm{L}} = 1.73$, and $n_{\mathrm{N}} = 3.19$.

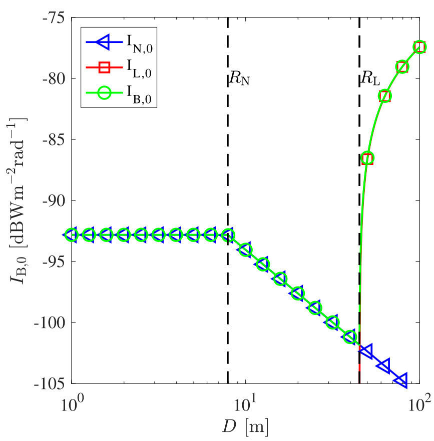

Fig. 4. An example of $I_{\mathrm{B},0}$, where $n_{\mathrm{L}} = 1.73$, and $n_{\mathrm{N}} = 3.19$.

more NLOS interference signals, and 2) to introduce less LOS interference signals. In the next section, practical criteria for the choice of the optimum ρ are presented.

IV. Energy Consumption of a Building

In this section, we use the maximum ratio between IGs of the BUD and a benchmark building as a FoM to evaluate the IG performance of the BUD. The obtained FoM is independent of P_{T}, the center frequency, the receiving threshold, and the position of the probe UE. The best ρ is obtained that maximizes the optimum IG ratio. Then we derive how much transmit power per coverage area P_{T} do we need to achieve the optimum IG ratio.

By inspection of Fig. 4 we can see that if a room satisfies the condition $P_D(d; x, y) = 0$ for any $D(\theta, x, y) > R_{\mathrm{N}}$, then the value of $I_{\mathrm{B},0}$ is independent of the layout of the building. From (3) and (16), we can then conclude that g_{I} is also independent of the building layout in this case.

Therefore, an *extremely small room*, with $P_D(d; x, y) = 0$ for any $D(\theta, x, y) > R_{\mathrm{N}}$, can be used as a new benchmark for interference gain evaluation. Hence, only NLOS interference needs to be accounted for to obtain the IG according to the following Lemma 1.

Lemma 1: For a small room with $P_D(d; x, y) = 0$ for any $D > R_{\mathrm{N}}$, the power of interference is computed by

$$I_{\mathrm{B,b}} = \frac{2\pi P_{\mathrm{th}} \rho^{\frac{2}{n_{\mathrm{N}}}}}{n_{\mathrm{N}} - 2}, \tag{19}$$

and the interference gain is computed by

$$g_{\mathrm{I,b}} = \begin{cases} \frac{(n_{\mathrm{N}}-2)\rho^{\frac{n_{\mathrm{N}}-2}{n_{\mathrm{N}}}}\left[1+2\ln\left(\frac{4\pi h_{\mathrm{T}} h_{\mathrm{R}}}{\sqrt{\rho}\lambda}\right)\right]}{2}, & 1 < \rho < \rho_{\mathrm{t}}, \\ \frac{2\pi(n_{\mathrm{N}}-2)\rho^{\frac{1}{2}-\frac{2}{n_{\mathrm{N}}}} h_{\mathrm{T}} h_{\mathrm{R}}}{\lambda}, & \rho \geq \rho_{\mathrm{t}}. \end{cases} \tag{20}$$

Proof: See Appendix B. ∎

A straightforward definition of the maximum IG ratio is

$$e_{\mathrm{I,s}} = \max_{\rho} \left\{ \mathrm{E}_{x,y} \left[\frac{g_{\mathrm{I}}(x, y)}{g_{\mathrm{I,b}}} \right] \right\}. \tag{21}$$

Substituting (3) into (21), we obtain

$$e_{\mathrm{I,s}} = \max_{\rho} \left\{ I_{\mathrm{B,b}} \mathrm{E}_{x,y} \left[I_{\mathrm{B}}^{-1}(x, y) \right] \right\}. \tag{22}$$

It follows then from (22) that the computation of $e_{\mathrm{I,s}}$ requires the computation of

$$\mathrm{E}_{x,y} \left[I_{\mathrm{B}}^{-1}(x, y) \right] = \mathrm{E}_{x,y} \left[\frac{1}{\int_0^{+\infty} I_{\mathrm{B},0}(d, \rho, n_{\mathrm{L}}, n_{\mathrm{N}}, P_{\mathrm{th}}) P_{D;x,y}(d; x, y) \mathrm{d}d} \right], \tag{23}$$

where $I_{\mathrm{B},0}$ and $P_{D;x,y}(d; x, y)$ are still coupled (i.e., both depend on the position of the probe UE) and are difficult to decoupled to ease the integration in (23). Also, the inverse moment of a random variable is in general not easy to compute [36]. Therefore, to facilitate the decoupling of network parameters and building parameters, we redefine the IG ratio by using the harmonic mean of $\frac{g_{\mathrm{I}}(x,y)}{g_{\mathrm{I,b}}}$, as follows.

Definition 1: Motivated by (21), the maximum IG ratio of building in terms of interference gain is defined as

$$e_{\mathrm{I}} = \max_{\rho} \left\{ \frac{1}{\mathrm{E}_{x,y} \left[\frac{g_{\mathrm{I,b}}}{g_{\mathrm{I}}(x,y)} \right]} \right\}. \tag{24}$$

The difference between the arithmetic mean $\mathrm{E}_{x,y}[\frac{g_{\mathrm{I}}(x,y)}{g_{\mathrm{I,b}}}]$ and the harmonic mean $\{\mathrm{E}_{x,y}[\frac{g_{\mathrm{I,b}}}{g_{\mathrm{I}}(x,y)}]\}^{-1}$ for our specific case is explained in Appendix C. (24) and (21) are compared in Fig. 5. In the computations, the considered room is rectangular, the center frequency is 28 GHz, $P_{\mathrm{T}} = -40$ dBWm^{-2}, and $P_{\mathrm{th}} = -110$ dBWm^{-2}. In Fig. 5, (24) is computed analytically by means of the closed-form expression of $P_D(d)$ given in the following Section V, whereas (21) is computed by averaging IG over uniformly distributed probe UEs. From Fig. 5, we conclude that behaviors of (24) and (21) match very well.

Therefore, in this paper, the maximum IG ratio definition given by (24) is adopted for computations for the entire building based on the LOS-distance PDF $P_D(d)$, which is decoupled from the wireless network parameters.

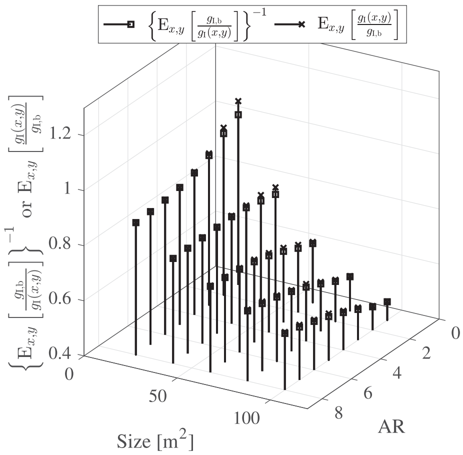

Fig. 5. Comparison between (24) and (21).

Substituting (3) into (24), we obtain

$$e_{\mathrm{I}} = \max_{\rho} \left\{ \frac{I_{\mathrm{B,b}}}{\mathrm{E}_{x,y}\left[I_{\mathrm{B}}(x,y)\right]} \right\}. \tag{25}$$

Thus, compared with $e_{\mathrm{I,s}}$, in the computation of e_{I} the expectation is only operated for $I_{\mathrm{B}}(x,y)$ over the space. Moreover, $I_{\mathrm{B},0}$ is independent of (x,y) in (16), and therefore, we will work on the expectation of $P_D(d;x,y)$ to simplification the computation of e_{I}.

Following some straightforward, but tedious, derivations, it can be shown that $\mathrm{E}_{x,y}[\frac{g_{\mathrm{I,b}}}{g_{\mathrm{I}}(x,y)}]$ is computed by (26) shown at the bottom of this page, where $P_D(d)$ is the LOS-distance PDF for the entire building defined as $P_D(d) = \mathrm{E}_{x,y}[P_D(d;x,y)]$. In the expectation computation, the probe UE is assumed to be uniformly distributed in the BUD.

The optimum ρ is then defined by

$$\rho_{\mathrm{o}} = \arg\max_{\rho} \left\{ \left\{ \mathrm{E}_{x,y}\left[\frac{g_{\mathrm{I,b}}}{g_{\mathrm{I}}(x,y)}\right] \right\}^{-1} \right\}. \tag{27}$$

Substituting (27) into (11), the optimum transmit power per coverage area is computed by

$$P_{\mathrm{T,o}} = \rho_{\mathrm{o}} P_{\mathrm{th}} \left(\frac{4\pi}{\lambda}\right)^2. \tag{28}$$

It is worth noting that the total transmit power of the extremely dense small-cell wireless network in this building will be obtained directly as $S_{\mathrm{A}} P_{\mathrm{T,o}}$ as long as we know the $P_{\mathrm{T,o}}$ of a building.

Theorem 1: Given the $P_D(d)$ of the BUD, the optimum ρ_{o} is the solution of the following equation

$$aA(D) - bB(D) + cC(D) = 0 \tag{29}$$

where

$$A(D) = \int_{\rho^{\frac{1}{n_L}}}^{+\infty} d^{2-n_L} P_D(d)\mathrm{d}d, \tag{30}$$

$$B(D) = \int_{\rho^{\frac{1}{n_L}}}^{+\infty} P_D(d)\mathrm{d}d, \tag{31}$$

$$C(D) = \int_{\rho^{\frac{1}{n_N}}}^{+\infty} d^{2-n_N} P_D(d)\mathrm{d}d, \tag{32}$$

$$a = \frac{n_N - 2}{n_N(2-n_L)}, \tag{33}$$

$$b = \frac{2n_L - 2n_N}{n_L n_N (2-n_L)} \rho^{\frac{2-n_L}{n_L}}, \tag{34}$$

$$c = \frac{1}{n_N}. \tag{35}$$

The values of $A(D)$, $B(D)$, and $C(D)$ depend on $P_D(d)$, i.e., an intrinsic building parameter. In general, $P_D(d)$ does not have an expression for a general room that is simple enough to have closed-form expressions for $A(D)$, $B(D)$, and $C(D)$. Even though for a rectangular room, $P_D(d)$ is still a piecewise function of d which is challenging to derive $A(D)$, $B(D)$, and $C(D)$ in closed-forms. Therefore, we use the bisection method [31, pp. 964–965] to solve it.

Proof: See Appendix D. ■

The maximum IG ratio of the BUD in terms of interference gain is then obtained substituting ρ_{o} into (26) and (24).

V. Computation of $P_D(d)$

Given the $P_D(d)$ of the BUD, the transmit power can be optimized through Theorem 1. In this section, we will present how to compute $P_D(d)$ when the layout of the building structures is provided.

For a BUD that consists of N_{r} rooms, $P_D(d)$ is computed using the law of total probability by

$$P_D(d) = \sum_{n_{\mathrm{r}}=1}^{N_{\mathrm{r}}} \frac{S_{n_{\mathrm{r}}} P_{D,n_{\mathrm{r}}}(d)}{S_{\mathrm{A}}}, \tag{36}$$

where $P_{D,n_{\mathrm{r}}}(d)$ denotes the LOS-distance PDF in the n_{r}th room, $S_{n_{\mathrm{r}}}$ denotes the area of the n_{r}th room, and $S_{\mathrm{A}} = \sum_{n_{\mathrm{r}}=1}^{N_{\mathrm{r}}} S_{n_{\mathrm{r}}}$ denotes the area of the BUD.

A. $P_{D,n_{\mathrm{r}}}(d)$ *for Arbitrarily Shaped Rooms*

In an irregular room, it is difficult to derive a closed-form expression for $P_{D,n_{\mathrm{r}}}(d)$. A feasible approach to obtain $P_{D,n_{\mathrm{r}}}(d)$ is the Monte Carlo method [30]. In this subsection, a Monte Carlo based random shoot algorithm (RSA) is proposed; the corresponding flow chart is shown in Fig. 6. Once launched, a set of N_{s} "shooters" with random positions is generated in the BUD. The position of the n_{s}th shooter is denoted as $(x_{n_{\mathrm{s}}}, y_{n_{\mathrm{s}}})$. For

$$\mathrm{E}_{x,y}\left[\frac{g_{\mathrm{I,b}}}{g_{\mathrm{I}}(x,y)}\right] = \frac{n_{\mathrm{N}}-2}{2-n_{\mathrm{L}}} \int_{R_{\mathrm{L}}}^{+\infty} \left(\rho^{\frac{n_{\mathrm{N}}-2}{n_{\mathrm{N}}}} d^{2-n_{\mathrm{L}}} - \rho^{\frac{2}{n_{\mathrm{L}}}-\frac{2}{n_{\mathrm{N}}}} \right) P_D(d)\mathrm{d}d + \int_{R_{\mathrm{N}}}^{+\infty} \rho^{\frac{n_{\mathrm{N}}-2}{n_{\mathrm{N}}}} d^{2-n_{\mathrm{N}}} P_D(d)\mathrm{d}d + \int_0^{R_{\mathrm{N}}} P_D(d)\mathrm{d}d \tag{26}$$

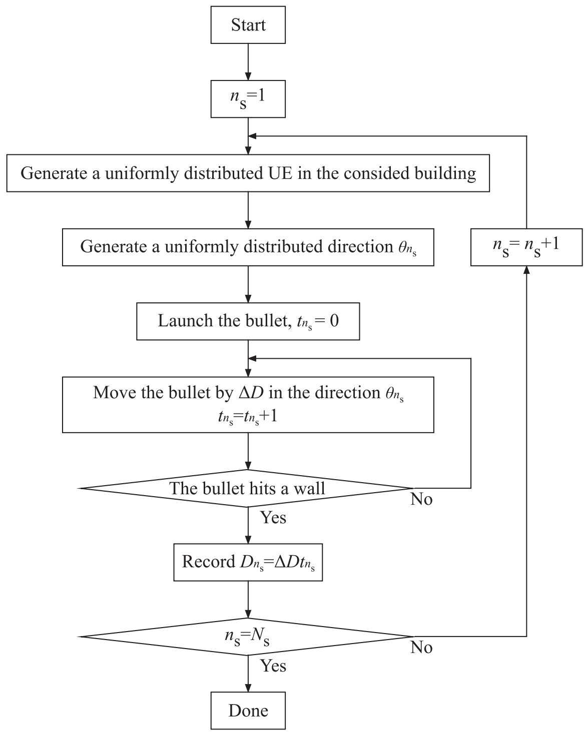

Fig. 6. Flowchart of the proposed random shoot algorithm.

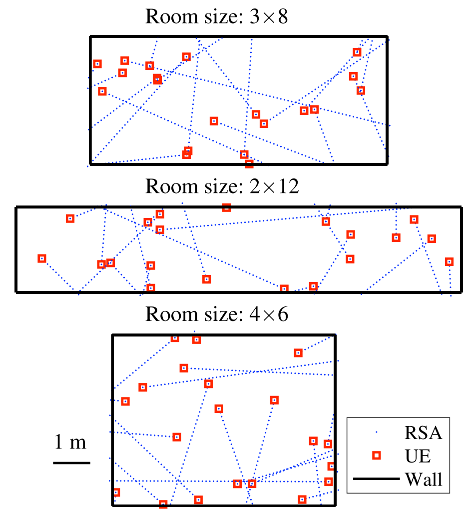

Fig. 7. Examples of the proposed random shoot algorithm with $N_s = 20$ and $\Delta D = 0.1$ m.

the n_sth shooter, a random shooting direction θ_{n_s} is allocated. x_{n_s}, y_{n_s}, and θ_{n_s} are uniformly distributed and independent for different shooters. For the first time step, each shooter shoots a bullet. Then, for each time step, every bullet repeatedly moves a distance ΔD in its shooting direction until it hits the obstacle. The fixed step size ΔD has to be small relative to the average D. As soon as the bullet from the n_sth shooter hits the wall, the number of the time steps t_{n_s} is recorded, and then we have a recorded $D_{n_s} = \Delta D t_{n_s}$.

With the database of the recorded D_{n_s}, the estimation of $P_{D,n_r}(d)$ is given by

$$\hat{P}_D(d) = \frac{1}{N_s}\sum_{n_s=1}^{N_s} \frac{u_{d-D_{n_s}-\frac{\Delta D}{2}}^{d-D_{n_s}+\frac{\Delta D}{2}}}{\Delta D}, \tag{37}$$

where

$$wu_a^b = u(D-b) - u(D-a). \tag{38}$$

In the numerical result section, the proposed RSA and (39) shown at the bottom of this page, are compared and validated.

B. $P_{D,n_r}(d)$ for Rectangular Rooms

In practical buildings, rectangular rooms are widely employed in building design. Fortunately, $P_{D,n_r}(d)$ for rectangular rooms has a simple closed-form expression. The $P_{D,n_r}(d)$ for one rectangular room with size $X \times Y$ is given by Theorem 2 below.

Theorem 2: The $P_{D,n_r}(d)$ for an $X \times Y$ rectangular room is computed by (39), where it is assumed that $Y \leq X$ and that the location of the probe UE (x, y) is uniformly distributed in the considered room. For a rectangular room with a size of $X \times Y$, $x \sim U(0, X)$ and $y \sim U(0, Y)$.

Proof: See Appendix E ■

Remark 3: Based on the outcome of Sections IV–V, an architect can use this model to evaluate the wireless energy efficiency of the BUD following the flowchart in Fig. 8.

VI. Numerical Results

In this section, we specialize our results to $n_L = 1.73$, and $n_N = 3.19$ following the 3GPP indoor channel model working at 0.5-100 GHz [27, Table 7.4.1-1].

A. Validations

For buildings tiled by 12×2, 8×3, and 6×4 rectangular rooms, the simulated and the analytic $P_{D,n_r}(d)$ is given in Fig. 9. The analytic $P_{D,n_r}(d)$ is computed by Theorem 2. The simulation results are obtained from the proposed RSA with $N_s = 10^7$ and $\Delta D = 10$ mm. It is observed that the analytic

$$P_{D,n_r}(d) = \begin{cases} \frac{2(X+Y-d)}{\pi XY}, & 0 \leq d < Y \\ \frac{2d-2\sqrt{d^2-Y^2}}{\pi dY}, & Y \leq d < X \\ \frac{2\,d^2-2Y\sqrt{d^2-X^2}-2X\sqrt{d^2-Y^2}}{\pi dXY}, & X \leq d < \sqrt{X^2+Y^2} \\ 0, & \sqrt{X^2+Y^2} < d \end{cases} \tag{39}$$

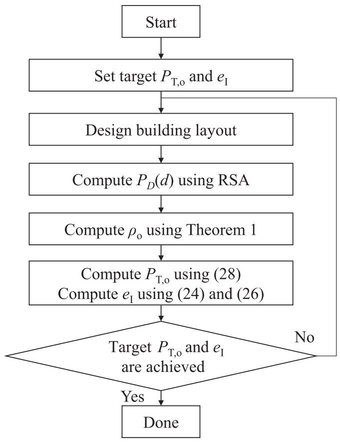

Fig. 8. Procedure of building design taking wireless energy efficiency into account.

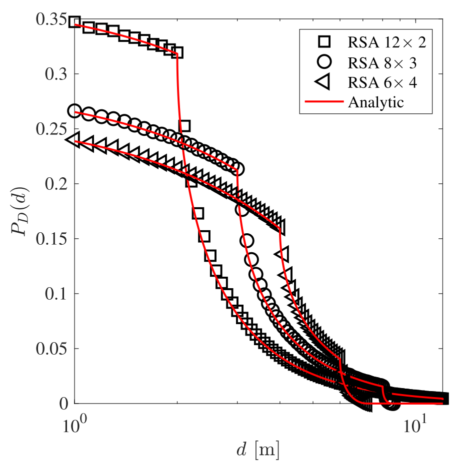

Fig. 9. Validation of $P_{D,n_{\mathrm{r}}}(d)$ for rectangular rooms.

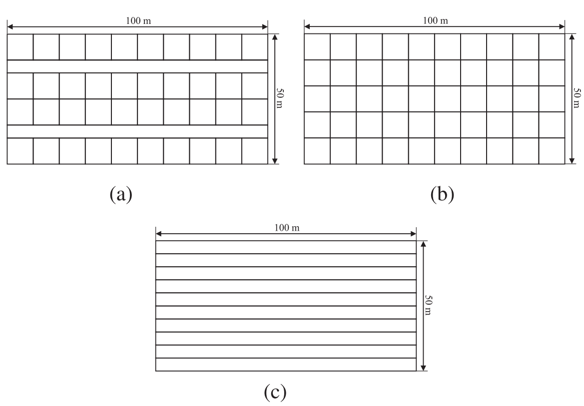

Fig. 10. Considered scenarios in numerical results. (a) WINNER II A1. (b) Pure room. (c) Pure corridor.

$P_{D,n_{\mathrm{r}}}(d)$ matches the simulations very well for rectangular rooms.

For the method validation, the layout of the WINNER II A1 indoor scenario [28], illustrated in Fig. 10(a), is taken as an example. The dimension of the building layout is 100 m $\times$ 50 m, and its area is $S_{\mathrm{A}} = 5000\ \mathrm{m}^2$. The building layout consists of 40 rooms, each of which has a size of 10 m $\times$ 10 m. The rooms are connected by two long corridors, each of which has a size of 5 m $\times$ 100 m. For comparison, we further investigate two extreme building layouts with $S_{\mathrm{A}} = 5000\ \mathrm{m}^2$, i.e., the pure-room scenario and the pure-corridor scenario, as shown in Figs. 10(b–c). As a validation, the simulated and the analytic $P_D(d)$ for above scenarios are given in Fig. 11. The simulation results are obtained from the proposed RSA with $N_{\mathrm{s}} = 10^7$, and the analytic result is computed by (36). It is observed that the analytic $P_D(d)$ matches the simulations very well.

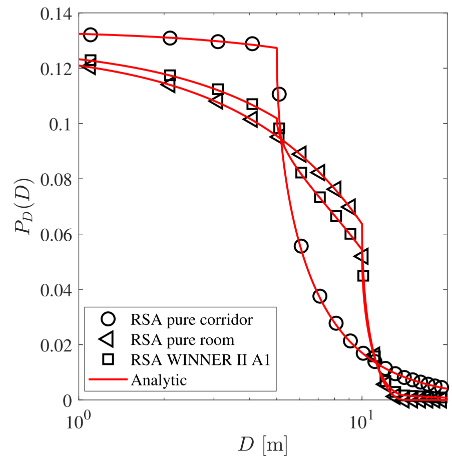

Fig. 11. Validation of $P_D(d)$ for the pure-corridor, the pure-room, and the WINNER II A1 scenario.

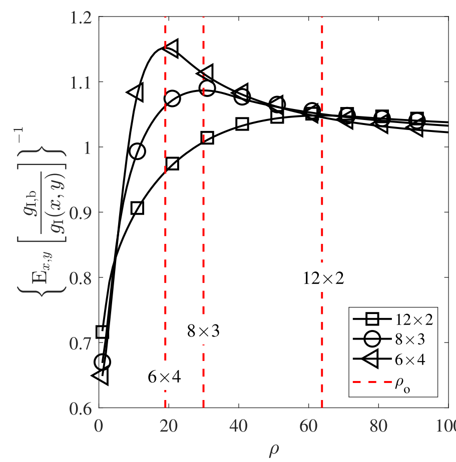

Fig. 12. Optimization of IG ratio for various room AR.

To validate the optimum ρ_{o}, the IG ratios are plotted against ρ in Figs. 12–13, where solid lines are computed by (26), and markers are obtained via simulations. The simulations are carried out by 10^5 simulating realizations of a PPP network with an intensity of $0.1\ \mathrm{BSs/m^2}$. A uniformly distributed UE is generated for each realization. In Fig. 12, the aspect ratio (AR) is the ratio of the width to height of the rectangular room. The IG ratio for various values of ρ is computed by (26) and ρ_{o} is computed by Theorem 1. Numerical results that ρ_{o} is capable to achieve the maximum IG ratio.

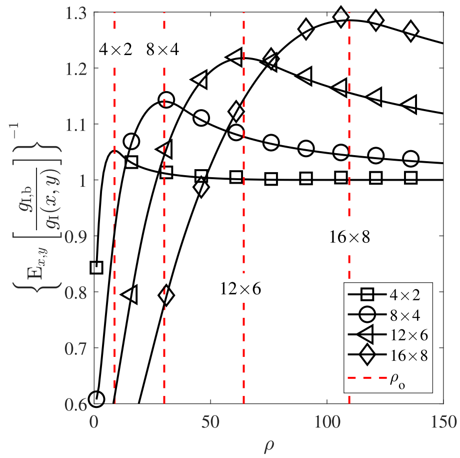

Fig. 13. Optimization of IG ratio for various room size.

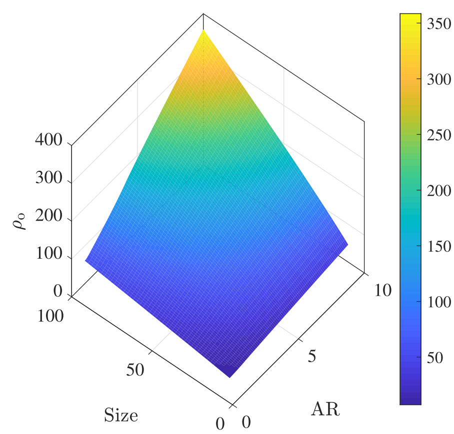

Fig. 14. Impact of room sizes and aspect ratios on ρ_o.

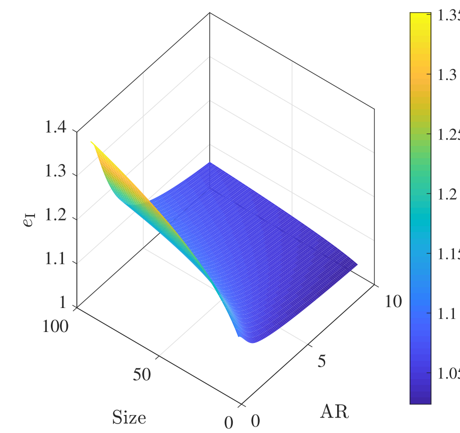

Fig. 15. Impact of room sizes and aspect ratios on the maximum IG ratio e_I.

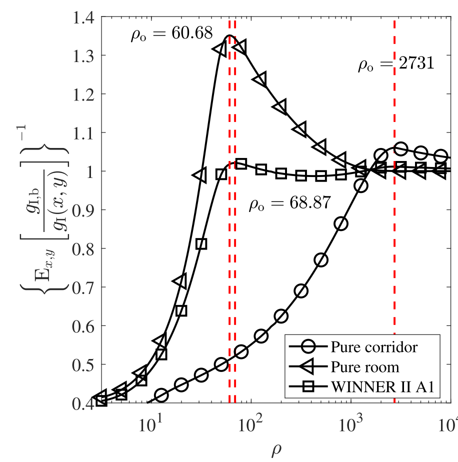

Fig. 16. Optimization of interference gain for the pure-corridor, the pure-room, and the WINNER II A1 indoor scenario.

B. Discussions

Impact of AR on ρ_o is plotted in Fig. 14, from which the following observations can be noted:

- For an increasing room size, ρ_o increases and therefore more power is required to achieve an optimum IG because an increasing R_L is required to reduce the power of the strong LOS interference signal.
- For a corridor with a larger AR, even though a fixed area is applied, strong LOS interference signal is more likely to appear in the long side direction. Therefore, more ρ_o is required to reduce the probability of $D > R_L$.

Impact of room sizes on the maximum IG ratio e_I is plotted in Fig. 15, from which it can be seen that

- For a larger room size, we use a larger ρ_o, and therefore, a larger e_I is obtained since more power is transmitted in total.
- However, an increasing AR introduces an increasing LOS interference power. Therefore, a larger ρ_o is used to balance the increased LOS interference power rather than to enhance the network performance. Therefore, a room with a large AR leads to large power consumption with lower wireless network performance.

A large e_I provides a better building wireless performance, and a smaller ρ_o indicates a less power consumption of a building. However, by changing the size of a room, e_I and ρ_o cannot be optimized simultaneously. A larger room has higher power consumption but better wireless performance. Nevertheless, an increasing AR reduces e_I and increases ρ_o simultaneously. During building design, architects are recommended to reduce ARs of rooms and corridors to save energy consumption by wireless networks.

The optimization of ρ assuming the WINNER II A1 indoor scenario is shown in Fig. 16, where solid lines are computed by (26), and markers are obtained via simulations. Numerical results show that in the WINNER II A1 indoor scenario $\rho_o = 68.87$. In this case we have that $R_L = 11.55$, and $R_N = 3.77$. Substituting $\rho_o = 68.87$ into (11), the required transmit power per coverage area obtained as shown in Fig. 17.

The pure-corridor scenario, the pure-room scenario, and the WINNER II A1 indoor scenario are compared in Fig. 16. Numerical results show that the pure-corridor scenario requires a significantly larger ρ_o than the WINNER II A1 scenario to achieve the optimum IG because corridors therein have a large AR. Whereas for the pure-room scenario, a slightly less ρ_o required than the WINNER II A1 indoor scenario. Moreover,

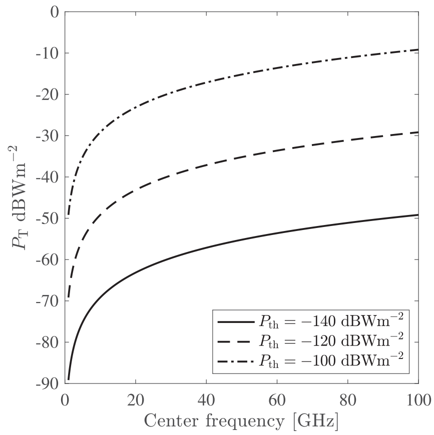

Fig. 17. Required transmitting power per coverage area in the WINNER II A1 indoor scenario.

the achievable IG ratio of the pure-room scenario is nearly 30% greater than that of the WINNER II A1 scenario. In summary, the pure-room scenario is more wireless-friendly than the WINNER II A1 scenario in terms of energy efficiency, but no passageway access is provided between rooms therein. In the building design stage, the function and the wireless performance of BUD need to be jointly considered.

From (28), we conclude that the optimum transmit power per coverage area for the WINNER II A1 indoor scenario is

$$P_{\rm T,o} = 68.87 P_{\rm th} \left(\frac{4\pi}{\lambda}\right)^2. \tag{40}$$

For an increasing operating frequency, the required $P_{\rm T}$ increases. When $P_{\rm th} = -120$ dBWm^{-2}, the optimum $P_{\rm T}$ at 1 GHz and 28 GHz are -69 dBWm^{-2} and -40 dBWm^{-2}, respectively.

As a final remark, it is worth noting that even if we have employed empirical propagation models in our theoretical derivations, it is only through actual measurements that the final verification of the proposed theoretical work can be achieved. Therefore, in the future, the theoretical predictions can strongly benefit from a comparison with actual measurement results.

VII. Conclusion

In this paper, contributions of building layouts and parameters of wireless networks are decoupled to separately analyze their contribution to interference gain (IG) of buildings. The maximum IG ratio of a building in terms of interference gain is defined in these conditions. Based on the provided definition of IG, the transmit power per coverage area is optimized by numerically solving an integral equation. Moreover, the fast optimization of the transmit power per coverage area facilitates green building design in terms of wireless power consumption. The standardized WINNER II A1 indoor scenario is exemplified to show the optimization process of transmit power per coverage area. To answer the question in the title of this paper, given the operating frequency wavelength λ and the sensitivity of receiver $P_{\rm th}$, the optimum transmit power per coverage area for the WINNER II A1 indoor layout is $P_{\rm T,o} = 68.87 P_{\rm th}(\frac{4\pi}{\lambda})^2$ dBWm^{-2}. Since the WINNER II A1 scenario has a floor area of 5000 m^2, to achieve a maximum IG ratio, the transmit power of extremely dense small network in this environment is $5000 \times P_{\rm T,o}$ W. Therefore, we conclude that the desired energy efficiency can be considerably improved if a building is designed by taking into account its wireless energy consumption at an early stage.

Appendix A
Proof of Proposition 1

Given $P_D(d)$, the total power of LOS and NLOS interference signals, $I_{\rm L}$ and $I_{\rm N}$, are computed by Lemma 2 and Lemma 3, respectively.

Lemma 2: Given the PDF $P_D(d)$, the total power of the LOS interference signals is computed by

$$I_{\rm L} = \frac{2\pi P_{\rm th}\rho \int_0^\infty u\left[d - \rho^{\frac{1}{n_{\rm L}}}\right] d^{2-n_{\rm L}} P_D(d){\rm d}d}{2 - n_{\rm L}} - \frac{2\pi P_{\rm th}\rho \int_0^\infty u\left[d - \rho^{\frac{1}{n_{\rm L}}}\right] \rho^{\frac{2-n_{\rm L}}{n_{\rm L}}} P_D(d){\rm d}d}{2 - n_{\rm L}}. \tag{41}$$

Proof: According to the definition of $I_{\rm L}$, given a probe UE at position (x, y), $I_{\rm L}(x, y)$ is derived from (42) shown at the bottom of this page. Since the probe UE is assumed to be uniformly distributed within the BUD, $I_{\rm L}$ is the expectation of $I_{\rm L}(x, y)$ over random variables x and y, i.e., (43) shown at the bottom of this page.

If the room is infinitely large, it is observed from (41) that $P_D(d) = \delta(d - \infty)$ and all interference links are LOS. Under this situation, $I_{\rm B} = I_{\rm L} = \infty$ if $n_{\rm L} < 2$, and thus $g_{\rm I} = 0$ according to (3), which is an extremely bad case. This result is

$$I_{\rm L}(x, y) = \int_0^{2\pi} \int_{R_{\rm L}}^{D(\theta,x,y)} P_{\rm T} G_{\rm L}(R) u(D(\theta, x, y) - R_{\rm L}) R{\rm d}R{\rm d}\theta \tag{42}$$

$$\begin{aligned} I_{\rm L} &= {\rm E}_{x,y}\left[\int_0^{2\pi} \int_{R_{\rm L}}^{D(\theta,x,y)} P_{\rm T} G_{\rm L}(R) u(D(\theta, x, y) - R_{\rm L}) R{\rm d}R{\rm d}\theta\right] \\ &= \frac{2\pi P_{\rm th}\rho}{2 - n_{\rm L}} \int_0^{2\pi} \frac{1}{2\pi} {\rm E}_{x,y}\left\{u\left[D(\theta, x, y) - R_{\rm L}\right]\left[D^{2-n_{\rm L}}(\theta, x, y) - {R_{\rm L}}^{2-n_{\rm L}}\right]\right\} {\rm d}\theta \end{aligned} \tag{43}$$

consistent with the results in PPP distributed small cells. Therein, the SIR is always equal to zero and thus the coverage rate is zero.

Considering θ as an uniformly distributed random variable with a PDF of

$$P_\theta = \begin{cases} \frac{1}{2\pi} & 0 < \theta < 2\pi \\ 0 & \text{else} \end{cases} \tag{44}$$

$$I_{\mathrm{L}} = \frac{2\pi P_{\mathrm{th}}\rho}{2-n_{\mathrm{L}}}\mathrm{E}_{(\theta,x,y)} \times \left\{u\left[D(\theta,x,y)-R_{\mathrm{L}}\right]\left[D^{2-n_{\mathrm{L}}}(\theta,x,y)-{R_{\mathrm{L}}}^{2-n_{\mathrm{L}}}\right]\right\}. \tag{45}$$

we then get (45). Since D is determined by θ, x, and y, $\mathrm{E}_{(\theta,x,y)}$ is equivalent to $\mathrm{E}_{D(\theta,x,y)}$. Given the PDF of D for random (θ,x,y), i.e., $P_D(d)$, (45) is rewritten as (41) and the proof is completed. ■

Lemma 3: Given the PDF $P_D(d)$, the total power of NLOS interference signals is computed by

$$I_{\mathrm{N}} = \frac{2\pi P_{\mathrm{th}}\rho\int_0^\infty \max\left\{D,\rho^{\frac{1}{n_{\mathrm{N}}}}\right\}^{2-n_{\mathrm{N}}} P_D(d)\mathrm{d}d}{n_{\mathrm{N}}-2}. \tag{46}$$

Proof: Given a probe UE at position (x,y), $I_{\mathrm{N}}(x,y)$ is given by

$$I_{\mathrm{N}}(x,y) = \int_0^{2\pi}\int_{\max\{R_{\mathrm{L}},D(\theta,x,y)\}}^{+\infty} P_{\mathrm{T}}G_{\mathrm{N}}(R)R\mathrm{d}R\mathrm{d}\theta. \tag{47}$$

Then, I_{N} is the expectation of $I_{\mathrm{N}}(x,y)$, i.e.,

$$I_{\mathrm{N}} = \frac{2\pi P_{\mathrm{th}}\rho}{2-n_{\mathrm{L}}}\int_0^{2\pi}\frac{1}{2\pi}\mathrm{E}_{x,y}\left\{\max\left\{D,\rho^{\frac{1}{n_{\mathrm{N}}}}\right\}^{2-n_{\mathrm{N}}}\right\}\mathrm{d}\theta. \tag{48}$$

By using (44), we obtain

$$I_{\mathrm{N}} = \frac{2\pi P_{\mathrm{th}}\rho}{2-n_{\mathrm{L}}}\mathrm{E}_{(\theta,x,y)}\left\{\max\left\{D,\rho^{\frac{1}{n_{\mathrm{N}}}}\right\}^{2-n_{\mathrm{N}}}\right\}. \tag{49}$$

Given $P_D(d)$, (49) is rewritten as (46) and the proof is completed. ■

Substituting (41) and (46) into $I_{\mathrm{B}} = I_{\mathrm{L}} + I_{\mathrm{N}}$, we obtain (16) and the proof is completed.

Appendix B
Proof of Lemma 1

For a small room with $P_D(d) = 0$ for any $D > R_{\mathrm{N}}$, we have

$$I_{\mathrm{B,b}} = \int_0^{R_{\mathrm{N}}} I_{\mathrm{B},0}(d,\rho,n_{\mathrm{L}},n_{\mathrm{N}})P_D(d)\mathrm{d}d. \tag{50}$$

Substituting (18) into (50), we have

$$I_{\mathrm{B,b}} = \int_0^{R_{\mathrm{N}}}\frac{2\pi P_{\mathrm{th}}\rho^{\frac{2}{n_{\mathrm{N}}}}}{n_{\mathrm{N}}-2}P_D(d)\mathrm{d}d = \frac{2\pi P_{\mathrm{th}}\rho^{\frac{2}{n_{\mathrm{N}}}}}{n_{\mathrm{N}}-2}\int_0^{R_{\mathrm{N}}}P_D(d)\mathrm{d}d. \tag{51}$$

Since $P_D(d)$ is a PDF, we have $\int_0^{R_{\mathrm{N}}} P_D(d)\mathrm{d}d = 1$, and therefore we obtain (19). By substituting (13) and (19) into (3), we obtain (20).

Appendix C
Difference Between the Arithmetic Mean and the Harmonic Mean

According to (21), denoting $R_{\mathrm{g}}(x,y) = \frac{g_{\mathrm{I,b}}}{g_{\mathrm{I}}(x,y)}$, we rewrit the arithmetic mean as

$$\mathrm{E}_{x,y}\left[\frac{g_{\mathrm{I}}(x,y)}{g_{\mathrm{I,b}}}\right] = \mathrm{E}_{x,y}\left[\frac{1}{R_{\mathrm{g}}(x,y)}\right]. \tag{52}$$

When the probe UE is randomly distributed in the considered room, R_{g} becomes a random variable with its PDF denoted by $P_{R_{\mathrm{g}}}(r)$, and its expected value $\mu = \mathrm{E}[R_{\mathrm{g}}]$. However, the mapping from (x,y) to R_{g} is too complicated for the derivation of $P_{R_{\mathrm{g}}}(r)$.

By using $P_{R_{\mathrm{g}}}(r)$, (52) is rewritten by

$$\mathrm{E}_{x,y}\left[\frac{g_{\mathrm{I}}(x,y)}{g_{\mathrm{I,b}}}\right] = \int_0^{+\infty}\frac{1}{r}P_{R_{\mathrm{g}}}(r)\mathrm{d}r. \tag{53}$$

Using Taylor series at μ, we have

$$\frac{1}{r} = \frac{1}{\mu} + \sum_{n=1}^{+\infty}\frac{(-1)^n}{n!\mu^{n+1}}(r-\mu)^n. \tag{54}$$

Substituting (54) into (53), we obtain

$$\mathrm{E}_{x,y}\left[\frac{g_{\mathrm{I}}(x,y)}{g_{\mathrm{I,b}}}\right] = \frac{1}{\mathrm{E}_{x,y}\left[\frac{g_{\mathrm{I,b}}}{g_{\mathrm{I}}(x,y)}\right]} + e, \tag{55}$$

where the difference

$$e = \mathrm{E}_{x,y}\left[\sum_{n=1}^{+\infty}\frac{(-1)^n}{n!\mu^{n+1}}(r-\mu)^n\right]. \tag{56}$$

In some previous works, e.g. [37, Eq. (24)], the difference e was omitted.

Appendix D
Proof of Theorem1

Substituting (20) into (24), we have

$$\rho_{\mathrm{o}} = \arg\min_\rho\left\{\int_0^{+\infty}K(d,\rho)P_D(d)\mathrm{d}d\right\}, \tag{57}$$

where the integral can be considered as an integral transform with a kernel $K(D,\rho)$, which is defined by

$$K(D,\rho) = u_0^{\rho^{\frac{1}{n_{\mathrm{N}}}}} + u_{\rho^{\frac{1}{n_{\mathrm{N}}}}}^{+\infty}D^{2-n_{\mathrm{N}}}\rho^{\frac{n_{\mathrm{N}}-2}{n_{\mathrm{N}}}} + \frac{n_{\mathrm{N}}-2}{2-n_{\mathrm{L}}}u_{\rho^{\frac{1}{n_{\mathrm{L}}}}}^{+\infty}\left(D^{2-n_{\mathrm{L}}}\rho^{\frac{n_{\mathrm{N}}-2}{n_{\mathrm{N}}}} - \rho^{\frac{2n_{\mathrm{N}}-2n_{\mathrm{L}}}{n_{\mathrm{L}}n_{\mathrm{N}}}}\right). \tag{58}$$

From (57), we observe that

- $K(D,\rho)$ is determined by network parameters ρ, n_{L}, and n_{N}, but these are independent of the layout of the building under design.
- $P_D(d)$ is determined by the layout of buildings, but of the wireless network parameters.

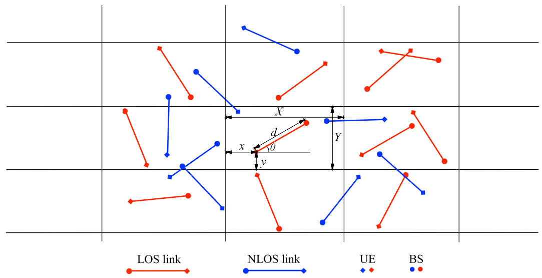

Fig. 18. Examples of random links with length d in a floor tiled by rectangular rooms.

To minimize (57), we need to find ρ that is the solution of the equation

$$\frac{\partial \int_0^{+\infty} K(d,\rho) P_D(d) \mathrm{d}d}{\partial \rho} = 0. \tag{59}$$

Exchange the order of the integral and the derivative, we have

$$\int_0^{+\infty} \frac{\partial K(d,\rho)}{\partial \rho} P_D(d) \mathrm{d}d = 0. \tag{60}$$

From (58), we have $\frac{\partial K(D,\rho)}{\partial \rho}$ as (61) shown at the bottom of this page. Substituting (61) into (60), we obtain (29).

Appendix E
Proof of Theorem 2

A. Computation of $P_D(d)$

Lemma 4: In a rectangular room with a size of $X \times Y$, $P_D(d)$ is computed by

$$P_D(d) = -\frac{\mathrm{d}F_D(d)}{\mathrm{d}d} \tag{62}$$

where $F_D(d)$ is the LOS probability of a link with a length d, in a floor tiled by rectangular rooms of side lengths X and Y, as shown in Fig. 18 .

Proof: Since PDF is the differentiation of CDF, we have

$$P_D(d) = \frac{\mathrm{d}\Pr\left[D < d\right]}{\mathrm{d}d}. \tag{63}$$

Substitute $\Pr[D < d] = 1 - \Pr[D \geq d]$ into (63), we have

$$P_D(d) = -\frac{\mathrm{d}\Pr\left[d \leq D\right]}{\mathrm{d}d}. \tag{64}$$

Considering the diagram in Fig. 18, the link with a length d is in a random position and direction on the floor. Then the event $d \leq D$ is equivalent to the event that the link between the transmitter and the receiver crosses neither horizontal nor vertical walls, i.e., the random link is a LOS link. By letting $F_D(d)$ denote the LOS probability, we obtain (62). ∎

It should be noted that computing the LOS probability $F_D(d)$ for the scenario represented in Fig. 18 can be interpreted as a conventional Laplace's extension of the Buffon needle problem [18], [29]. The computations are shown next.

Assuming uniformly distributed links, the joint PDF of (x, y, θ) is given by

$$P_{(x,y,\theta)} = \begin{cases} \frac{2}{\pi XY}, & 0 < x < X, 0 < y < Y, 0 < \theta < \frac{\pi}{2}. \\ 0, & \text{else}. \end{cases} \tag{65}$$

When $d > \sqrt{X^2 + Y^2}$, the link is impossible to be LOS and $F_D(d) = 0$. Under conditions $d < Y$, $Y \leq d < X$ and $X \leq d < \sqrt{X^2 + Y^2}$, $F_D(d)$ has different expressions which are derived as follows.

B. $d < Y$

When $d < Y$, the link is LOS only if

$$\begin{cases} x + d\sin\theta < X, \\ y + d\sin\theta < Y, \\ 0 < \theta < \frac{\pi}{2}. \end{cases} \tag{66}$$

Therefore,

$$\begin{aligned} F_D(d) &= \int_0^{\frac{\pi}{2}} \int_0^{X - d\cos\theta} \int_0^{Y - d\sin\theta} \frac{1}{\frac{\pi}{2}XY} \mathrm{d}x\mathrm{d}y\mathrm{d}\theta \\ &= \frac{\pi XY - 2d(X+Y) + d^2}{\pi XY}, \end{aligned} \tag{67}$$

and following (62), we have

$$P_D(d) = \frac{2(X + Y - d)}{\pi XY}. \tag{68}$$

C. $Y \leq d < X$

When $Y \leq d < X$, the link is LOS only if

$$\begin{cases} x + d\sin\theta < X \\ y + d\sin\theta < Y \\ 0 < \theta < \arcsin\left(\frac{Y}{d}\right) \end{cases} \tag{69}$$

Therefore, $F_D(d)$ is computed by (70) shown at the bottom of this page. Following (62), we have

$$P_D(d) = \frac{2\left(d - \sqrt{d^2 - Y^2}\right)}{\pi d Y} \tag{71}$$

$$\frac{\partial K(D,\rho)}{\partial \rho} = \frac{n_N - 2}{2 - n_L} u_{\rho^{\frac{1}{n_L}}}^{+\infty} \left(\frac{n_N - 2}{n_N} D^{2-n_L} \rho^{-\frac{2}{n_N}} - \frac{2n_N - 2n_L}{n_L n_N} \rho^{\frac{2n_N - 2n_L - n_N n_L}{n_N n_L}} \right) + \frac{n_N - 2}{n_N} u_{\rho^{\frac{1}{n_N}}}^{+\infty} D^{2-n_N} \rho^{-\frac{2}{n_N}} \tag{61}$$

$$F_D(d) = \int_0^{\arcsin\left(\frac{Y}{d}\right)} \int_0^{X - d\cos\theta} \int_0^{Y - d\sin\theta} \frac{1}{\frac{\pi}{2}XY} \mathrm{d}x\mathrm{d}y\mathrm{d}\theta = \frac{2\left[XY \arcsin\left(\frac{Y}{d}\right) - \frac{Y^2}{2} + X\sqrt{d^2 - Y^2} - Xd\right]}{\pi XY} \tag{70}$$

$$F_D(d) = \int_{\arccos\left(\frac{X}{d}\right)}^{\arcsin\left(\frac{Y}{d}\right)} \int_0^{X-d\cos\theta} \int_0^{Y-d\sin\theta} \frac{1}{\frac{\pi}{2}XY} \mathrm{d}x\mathrm{d}y\mathrm{d}\theta$$
$$= \frac{2XY\left[\arcsin\left(\frac{Y}{d}\right) - \arccos\left(\frac{X}{d}\right)\right] - \left(X^2+Y^2+d^2\right) + 2Y\sqrt{d^2-X^2} + 2X\sqrt{d^2-Y^2}}{\pi XY}. \quad (73)$$

D. $X \leq d < \sqrt{X^2+Y^2}$

When $X \leq d < \sqrt{X^2+Y^2}$, the link is LOS only if

$$\begin{cases} x + d\sin\theta < X, \\ y + d\sin\theta < Y, \\ \arccos\left(\frac{X}{d}\right) < \theta < \arcsin\left(\frac{Y}{d}\right). \end{cases} \quad (72)$$

Therefore, $F_D(d)$ is computed by (73) shown at the top of this page. Following (62), we have

$$P_D(d) = \frac{2\ d^2 - 2Y\sqrt{d^2-X^2} - 2X\sqrt{d^2-Y^2}}{\pi dXY}. \quad (74)$$

Combining (68), (71), and (74), we obtain (39).

References

[1] H. Jiang, C. Cai, X. Ma, Y. Yang, and J. Liu, "Smart home based on WiFi sensing: A survey," *IEEE Access*, vol. 6, pp. 13317–13325, 2018.

[2] X. Wang, M. Umehira, H. Otsu, T. Kawatani, and S. Takeda, "Energy efficient learning-based indoor multi-band WLAN for smart buildings," *IEEE Access*, vol. 6, pp. 34324–34333, 2018.

[3] T. Nam and T. A. Pardo, "Conceptualizing smart city with dimensions of technology, people, and institutions," in *Proc. Annu. Int. Conf. Digit. Government Res.*, 2011, pp. 282–291.

[4] V. Chandrasekhar, J. G. Andrews, and A. Gatherer, "Femtocell networks: A survey," *IEEE Commun. Mag.*, vol. 46, no. 9, pp. 59–67, Sep. 2008.

[5] J. G. Andrews *et al.*, "What will 5G be?" *IEEE J. Sel. Area Commun.*, vol. 32, no. 6, pp. 1065–1082, Jun. 2014.

[6] X. Ge, S. Tu, G. Mao, C. Wang, and T. Han, "5G ultra-dense cellular networks," *IEEE Wireless Commun.*, vol. 23, no. 1, pp. 72–79, Feb. 2016.

[7] I. Hwang, B. Song, and S. S. Soliman, "A holistic view on hyper-dense heterogeneous and small cell networks," *IEEE Commun. Mag.*, vol. 51, no. 6, pp. 20–27, Jun. 2013.

[8] X. Ge, J. Yang, H. Gharavi, and Y. Sun, "Energy efficiency challenges of 5G small cell networks," *IEEE Commun. Mag.*, vol. 55, no. 6, pp. 184–191, May 2017.

[9] K. Haneda, J. Jarvelainen, A. Khatun, and K. Takizawa, "Spatial coexistence of millimeter-wave distributed indoor channels," in *Proc. IEEE VTC-Spring*, 2015, pp. 1–5.

[10] L. Azpilicueta, F. Falcone, and R. Janaswamy, "A hybrid ray launching-diffusion equation approach for propagation prediction in complex indoor environments," *IEEE Antennas Wireless Propag. Lett.*, vol. 16, pp. 214–217, 2017.

[11] P. Tseng, Y. Chan, Y. Lin, D. Lin, N. Wu, and T. Wang, "Ray-tracing-assisted fingerprinting based on channel impulse response measurement for indoor positioning," *IEEE Trans. Instrum. Meas.*, vol. 66, no. 5, pp. 1032–1045, May 2017.

[12] F. Casino, L. Azpilicueta, P. Lopez-Iturri, E. Aguirre, F. Falcone, and A. Solanas, "Optimized wireless channel characterization in large complex environments by hybrid ray launching-collaborative filtering approach," *IEEE Antennas Wireless Prop. Lett.*, vol. 16, pp. 780–783, 2017.

[13] K. A. Remley, H. R. Anderson, and A. Weisshar, "Improving the accuracy of ray-tracing techniques for indoor propagation modeling," *IEEE Trans. Veh. Tech.*, vol. 49, no. 6, pp. 2350–2358, Nov. 2000.

[14] dS. S. Zhekov, O. Franek, and G. F. Pedersen, "Numerical modeling of indoor propagation using FDTD method with spatial averaging," *IEEE Trans. Veh. Tech.*, vol. 67, no. 9, pp. 7984–7993, Sep. 2018.

[15] M. K. Müller, M. Taranetz, and M. Rupp, "Analyzing wireless indoor communications by blockage models," *IEEE Access*, vol. 5, pp. 2172–2186, 2017.

[16] S. Niknam, B. Natarajan, and R. Barazideh, "Interference analysis for finite-area 5G mmWave networks considering blockage effect," *IEEE Access*, vol. 6, pp. 23470–23479, 2018.

[17] A. K. Gupta, J. G. Andrews, and R. W. Heath, "Macrodiversity in cellular networks with random blockages," *IEEE Trans. Wireless Commun.*, vol. 17, no. 2, pp. 996–1010, Feb. 2018.

[18] H. Zheng, J. Zhang, H. Li, Q. Hong, H. Hu, and J. Zhang, "Exact line-of-sight probability for channel modelling in typical indoor environments," *IEEE Antennas Wireless Propag. Lett.*, vol. 17, no. 7, pp. 1359–1362, Jul. 2018.

[19] T. Bai, R. Vaze, and R. W. Heath, "Analysis of blockage effects on urban cellular networks," *IEEE Trans. Wireless Commun.*, vol. 13, no. 9, pp. 5070–5083, Sep. 2014.

[20] B. Mondal *et al.*, "3D channel model in 3GPP," *IEEE Commun. Mag.*, vol. 53, no. 3, pp. 16–23, Mar. 2015.

[21] W. Yang, J. Zhang, and J. Zhang, "Machine learning based indoor line-of-sight probability prediction," in *Proc. IEEE Int. Symp. Antennas Propag.*, 2019, pp. 1–3.

[22] J. Zhang *et al.*, "Evaluating the wireless performance of a building," U.K. Patent, 1810995.9, 2018

[23] EUROSTARS Project 11088 BuildWise (The development of a software tool to design buildings with tailored wireless performance), 2017. [Online]. Available: https://www.eurostars-eureka.eu/project/id/11088

[24] C. Sommer and F. Dressler, "Using the right two-ray model? A measurement based evaluation of PHY models in VANETs," in *Proc. ACM MobiCom*, 2011, pp. 1–3.

[25] X. Zhang and J. Andrews, "Downlink cellular network analysis with multi-slope path loss models," *IEEE Trans. Commun.*, vol. 63, no. 5, pp. 1881–1894, May 2015.

[26] S. Sun *et al.*, "Investigation of prediction accuracy, sensitivity, and parameter stability of large-scale propagation path loss models for 5G wireless communications," *IEEE Trans. Veh. Tech.*, vol. 65, no. 5, pp. 2843–2860, May 2016.

[27] 3GPP, "Study on channel model for frequencies from 0.5 to 100 GHz," Sophia Antipolis Cedex, France, TR 38.901 version 14.0.0 Release 14, 2017.

[28] J. Meinilä *et al.*, "WINNER II channel models," *Radio Tech. Concepts MT-Advanced*, pp. 39–92, 2009.

[29] B. Arnow, "On Laplace's extension of the Buffon needle problem," *College Math. J.*, vol. 25, no. 1, pp. 40–43, 1994.

[30] N. Metropolis, and S. Ulam, "Monte Carlo method," *J. Amer. Statistical Assoc.*, vol. 44, pp. 335–341, 1949.

[31] G. Arfken, *Mathematical Methods for Physicists*, 3rd ed. Orlando, FL, USA: Academic, 1985.

[32] B. Yang, G. Mao, M. Ding, X. Ge, and X. Tao, "Dense small cell networks: From noise-limited to dense interference-limited," *IEEE Trans. Veh. Tech.*, vol. 67, no. 5, pp. 4262–4277, May 2018.

[33] J. G. Andrews, F. Baccelli, and R. K. Ganti, "A tractable approach to coverage and rate in cellular networks," *IEEE Trans. Commun.*, vol. 59, no. 11, pp. 3122–3134, Nov. 2011.

[34] J. Park, N. Lee, J. G. Andrews, and R. W. Heath, "On the optimal feedback rate in interference-Limited multi-antenna cellular systems," *IEEE Trans. Wireless Commun.*, vol. 15, no. 8, pp. 5748–5762, Aug. 2016.

[35] M. Min, "Bounds on the optimal feedback rate for multi-antenna systems in interference-limited cellular networks," *IEEE Trans. Wireless Commun.*, vol. 17, no. 7, pp. 4845–4860, Jul. 2018.

[36] S. Sung, "On inverse moments for a class of nonnegative random variables," *J. Inequalities Appl.*, vol. 2010, 2010, Art. no. 823767.

[37] A. R. Elsherif, Z. Ding, and X. Liu, "Dynamic MIMO precoding for femtocell interference mitigation," *IEEE Trans. Commun.*, vol. 62, no. 2, pp. 648–666, Feb. 2014.

Jiliang Zhang (Senior Member, IEEE) received the B.E., M.E., and Ph.D. degrees from the Harbin Institute of Technology, Harbin, China, in 2007, 2009, and 2014, respectively. He was a Postdoctoral Fellow with Shenzhen Graduate School, Harbin Institute of Technology from 2014 to 2016, an Associate Professor with the School of Information Science and Engineering, Lanzhou University from 2017 to 2019, and a Researcher with the Department of Electrical Engineering, Chalmers University of Technology, Gothenburg, Sweden from 2017 to 2018. He is currently a Marie Curie Research Fellow with the Department of Electronic and Electrical Engineering, The University of Sheffield, Sheffield, U.K. His current research interests include, but are not limited to wireless channel modelling, modulation system, relay system, wireless ranging system, vehicular communications, ultra-dense small cell networks, neural dynamic, and smart environment modeling.

Andrés Alayón Glazunov (Senior Member, IEEE) was born in Havana, Cuba. He received the M.Sc. (Engineer-Researcher) degree in physical engineering from Peter the Great St. Petersburg Polytechnic University (Polytech), St. Petersburg, Russia, in 1994, the Ph.D. degree in electrical engineering from Lund University, Lund Sweden, in 2009, and the Docent (Habilitation) qualification in antenna systems from the Chalmers University of Technology, Gothenburg, Sweden, in 2017. From 1996 to 2005, he held various research and specialist positions in the Telecom industry, e.g., Ericsson Research, Telia Research, and TeliaSonera, in Stockholm, Sweden. From 2001 to 2005, he was the Swedish delegate to the European Cost Action 273 and from 2018 to 2020 he was the Dutch delegate to the European Cost Action IRACON. He has been one of the pioneers in producing the first standardized OTA measurement techniques for 3GPP, and devising novel OTA techniques, e.g., the Random-LOS and the Hybrid antenna characterization setups. He has contributed to, or initiated various European research projects, e.g., more recently, the is3DMIMO, the WAVECOMBE and the Build-Wise projects under the auspices of the H2020 European Research and Innovation program. He has also contributed to the international 3GPP and the ITU standardization bodies. From 2009 to 2010, he held a Marie Curie Senior Research Fellowship at the Centre for Wireless Network Design, University of Bedfordshire, Luton, U.K. From 2010 to 2014, he held a postdoctoral position with the Electromagnetic Engineering Laboratory, KTH-Royal Institute of Technology, Stockholm, Sweden. From 2014 to 2018, he held an Assistant Professor position with Chalmers University of Technology, Gothenburg, Sweden. He is currently an Associate Professor with the Department of Electrical Engineering, University of Twente, Enschede, the Netherlands, where he is leading the Radio, Propagation and Antenna Systems research. And he is also an Affiliate Professor with the Chalmers University of Technology, Gothenburg, Sweden, where he is leading the OTA Characterization of Antenna Systems research area. He is the author of more than hundred scientific and technical publications. He is the co-author and co-editor of the text book *LTE-Advanced and Next Generation Wireless Networks – Channel Modeling and Propagation* (Wiley, 2012). His current research interests include, but are not limited to mmWave array antenna design, MIMO antenna systems, electromagnetic theory, fundamental limitations on antenna-channel interactions, radio propagation channel measurements, modeling and simulations, wireless performance in the built environment, and the OTA characterization of antenna systems and wireless devices.

Jie Zhang (Senior Member, IEEE) has been held the Chair in Wireless Systems with the Department of Electronic and Electrical Engineering, University of Sheffield since January 2011. He is also Founder, Board Chairman, and Chief Scientific Officer (CSO) of Ranplan Wireless, a public company listed on Nasdaq OMX. Ranplan Wireless produces a suite of world leading indoor and the only joint indoor–outdoor 5G/4G/WiFi network planning and optimization tools suites including Ranplan Professional and Collaboration-Hub, which are being used by the world's largest mobile operators and network vendors across the globe. Along with his students and colleagues, he has pioneered research in small cell and heterogeneous network (HetNet) and authored some of the landmark papers and books on these topics, widely used by both academia and industry. He has authored some of the earliest papers on using social media network data for proactive network optimisation. Since 2010, he and his team have also developed ground-breaking work in modeling and designing smart built environments considering both wireless and energy efficiency. His Google scholar citations are in excess of 7000 with an H-index of 35. Prior to his current appointments, he studied and worked at Imperial College London, Oxford University, University of Bedfordshire, and East China University of Science and Technology, reaching the rank of a Lecturer, Reader and Professor in 2002, 2005, and 2006, respectively.